Combustion and Flame 227 (2021) 135–146

Contents lists available at ScienceDirect

Combustion and Flame

journal homepage: www.elsevier.com/locate/combustflame

Uncertainty analysis in mechanism reduction via active subspace and transition state analyses

Xingyu Su[a], Weiqi Ji[a], Zhuyin Ren[a,b,*]

[a] Center for Combustion Energy, Tsinghua University, Beijing 100084, China
[b] Institute for Aero Engine, Tsinghua University, Beijing 100084, China

ARTICLE INFO

Article history:
Received 19 March 2020
Revised 24 December 2020
Accepted 29 December 2020

Keywords:
Mechanism reduction
Uncertainty quantification
Active subspace
Transition state

ABSTRACT

A systematic approach is formulated for the uncertainty analysis of kinetic parameters on combustion characteristics during skeletal reduction. The active subspace method together with sensitivity analysis is first employed to identify extreme low-dimensional active subspace of input parameter space and to facilitate the construction of response surfaces with small size of samples. An intermediate transition state during reduction is then defined such that the uncertainty change arising from uncertainty parameter truncation and reaction coupling during reduction can be decoupled and quantified. The approach is demonstrated in the reduction of a 55-species, 290-reaction dimethyl ether (DME) mechanism, with the rate constants characterized by independent lognormal distribution. Three representative skeletal mechanisms are identified for the uncertainty analysis, with each of the subsequent reduction yielding significant errors in the single-stage and/or two-stage DME-air auto-ignition process. Results show that sensitivity analysis can reduce the number of kinetic parameters from 290 down to 32, and the active subspace method can further identify a dominant active direction within this 32-dimensional subspace, which greatly facilitates the polynomial fitting for constructing the response surface of the ignition delay times. The uncertainty analysis with the polynomial chaos expansion method shows that the reduction from DME42 with 42 species to DME40 with 40 species has influential effect on the high-temperature reaction pathway; while the reduction from DME55 to DME42 and from DME40 to DME30 mainly affects the low-temperature pathway. In addition, the uncertainty change associated with parameter truncation is shown to be proportional to the change in the most active direction, which could further accelerate uncertainty analysis.

1. Introduction

Predictive reacting flow simulations often require well-designed chemical kinetics models as a foundation. Over the past several decades, substantial advance of detailed chemical mechanisms for hydrocarbon fuels has been made, and the number of species and chemical reactions involved has dramatically increased with the corresponding increase in the complexity of fuel molecules considered [1]. Accuracy of such kinetic models can be assured, in principle, by systematic studies of individual rate coefficients. However, many sources embedded with experimental uncertainties in the rate parameters inevitably bring uncertainties into the kinetics models. The uncertainty quantification (UQ) of chemical kinetics on the prediction of quantities of interests (QoIs) such as ignition delay times (IDTs) and laminar flame speeds in simple reactors and flames have been systematically studied [2]. Response surface methods such as those in high dimensional model representation (HDMR) [3,4] and polynomial chaos expansion (PCE) [5,6] have been employed to accelerate the uncertainty quantification (UQ) process.

The propagation of kinetic uncertainty in mechanism reduction and the subsequent turbulent combustion simulations has been gaining increasing attention [7,8]. The presence of a large number of species and a wide range of chemical time scales makes it expensive to directly apply detailed mechanisms in multi-dimensional simulations. Skeletal mechanisms for hydrocarbon fuels, which consist of a small subset of species and reactions from detailed ones to capture the dominant reaction pathways, can now be systematically obtained through the methods of directed relation graph (DRG) [9], computational singular perturbation (CSP) [10], sensitivity analysis [11,12], etc. Over the past years, much attention has been drawn on the accuracy comparison for the

* Corresponding author at: Center for Combustion Energy, Tsinghua University, Beijing 100084, China.
E-mail address: zhuyinren@tsinghua.edu.cn (Z. Ren).

https://doi.org/10.1016/j.combustflame.2020.12.053
0010-2180/

QoIs, between the detailed and skeletal ones with fixed kinetic parameters.

In view of the above considerations, it is of both scientific and practical interests to investigate the dependence of uncertainty in the prediction of QoIs on the elimination of species and reactions during the reduction process; in other words, the dependence of uncertainty on the size of skeletal mechanisms. Xin et al. [8] first studied this dependence by analyzing the uncertainty change in the skeletal reduction of *n*-butane and *i*-butane mechanisms, in which sensitivity analysis is employed to identify the important reactions and thus reduce the number of kinetic parameters for propagating uncertainty. It is revealed that the uncertainty decreases monotonically with the model size only when the coupling among reactions is weak. Note that sensitivity analysis alone in [8] can only reduce the number of important kinetic parameters to 10–30, which is still computationally intractable as the computational models for QoIs are expensive. Moreover, the analysis with PCE coefficients employed cannot decouple the uncertainty sources from parameter truncation and reaction coupling explicitly.

In this study, the methods of active subspace and transition state analysis are proposed for the efficient and quantitative uncertainty analysis in mechanism reduction. The active subspace method together with sensitivity analysis is employed to identify low-dimensional active subspace of the input parameter space and to construct the response surface with sufficiently small size of samples. To quantify the uncertainty change during skeletal reduction, an intermediate "transition state" during reduction is defined, in which the truncated reactions are maintained but with their uncertainties in kinetic parameters being neglected, such that the uncertainty change is decoupled into contributions from parameter truncation and reaction coupling, respectively. That is, the transition state has the same set of species and reactions as the detailed one, but the kinetic parameters for the truncated reactions during reduction are fixed at the nominal values without accounting for uncertainties. The uncertainty analysis will be demonstrated in the skeletal reduction of a 55-species dimethyl ether (DME) mechanism [13].

2. Methodology

In this section, the four major components for uncertainty propagation in mechanism reduction are described. Skeletal reduction with DRG is first briefly reviewed for the generation of a series of skeletal mechanisms for uncertainty analysis, followed by the description of uncertainty characterization of kinetic parameters. The kinetic parameter reduction via active subspace method is then introduced to accelerate the uncertainty propagation from the parameter space to the QoI space. With uncertainties of the detailed and skeletal models acquired, the uncertainty analysis via transition state is elaborated in Section 2.4.

2.1. Skeletal mechanism reduction

The 55-species, 290-reaction dimethyl ether (DME) mechanism of Zhao et al. [13] is used as an example to illustrate the uncertainty analysis in mechanism reduction. In this study, mechanism reduction is performed at the nominal kinetic parameters, then the uncertainty propagations for the QoIs are analyzed among the mechanisms with different levels of details. That is, model reduction and model uncertainty analysis are decoupled for the convenience of analysis. It is also worth mentioning that this study is of practical interest for the mechanism reduction methods that account for model uncertainties since it is necessary to analyze uncertainty changes during the reduction process.

The DRG method [9] is employed to generate representative skeletal mechanisms of different sizes. Note that DME55 and the DRG method are employed for the convenience of demonstration, and the proposed approach is applicable to other detailed mechanisms and skeletal reduction methods. The DRG eliminates unimportant species through reaction flux analysis. For a given thermochemical state, the pair-wise correlation coefficient $r_{A,B}$ is calculated to quantify the influence of eliminating species B on the reaction rate of species A,

$$r_{AB} \equiv \frac{\max|\nu_{\mathrm{A},i}\omega_i\delta_{\mathrm{B},i}|}{\max|\nu_{\mathrm{A},i}\omega_i|} \tag{1}$$

$$\delta_{\mathrm{B},i} = \begin{cases} 1 & i\text{th reaction involves B} \\ 0 & \text{otherwise} \end{cases}$$

where ω_i is the net reaction rate of the ith reaction and $\nu_{\mathrm{A},i}$ is the stoichiometric coefficient of species A in the ith reaction. Species B is regarded as important to species A if $r_{AB} > \varepsilon_{DRG}$ and cannot be eliminated if species A is important. Species strongly coupled, to the user-specified search initiating or starting species, directly or indirectly, are retained in the skeletal mechanism. More algorithm details are given in [9].

Note that model uncertainty and model reduction are inherently coupled with each other if one also considers the uncertainties in kinetic parameters during mechanism reduction, as detailed in [14]. One possible approach for considering parameter uncertainties during DRG reduction is to generate samples in the parameter space and obtain a weighted r_{AB} with a proper filter. Then skeletal reduction can be performed based on the weighted r_{AB}. Recall that the focus of this study is not to formulate a reduction method that accounts for parameter uncertainty and mechanism reduction is currently performed at nominal kinetic parameters without accounting for their uncertainties.

The DRG method uses representative thermochemical data for reaction flux analysis, which may draw from solutions of auto-ignition, perfectly stirred reactors and laminar premixed flames etc., under relevant conditions [9]. In this study, the sample compositions for DRG reduction are obtained from the autoignition of DME/air mixtures with the DME55 mechanism covering the conditions of 650K$\leq T_0 \leq$1200 K, 1 atm $\leq p \leq$ 20 atm, and $0.5 \leq \phi \leq 1.5$. With a given reduction threshold ε_{DRG}, a skeletal mechanism consists of all the retained species and reactions from individual sample compositions. In the reduction process, the QoI considered is the ignition delay time (IDT) that has practical importance especially in internal combustion engines. DME is one of the simplest hydrocarbons exhibiting the negative temperature coefficient behavior [15-17]. It is employed for demonstrating the uncertainty propagation in the reduction of hydrocarbon mechanisms with complex dynamics. Note that even though the sample data from autoignition processes are employed for DRG reduction, the skeletal mechanisms obtained are also validated with laminar premixed flames in Section 3. The uncertainty analysis approach is general and could be applied to other reduction methods with different representative sample thermochemical data.

2.2. Uncertainty characterization of kinetic parameters

For homogeneous adiabatic, isochoric autoignition, the set of governing ordinary differential equations (ODEs) can be rewritten in a compact form as

$$\frac{d\boldsymbol{\varphi}}{dt} = \boldsymbol{F}(\boldsymbol{\varphi}; \boldsymbol{k}) \tag{2}$$

where $\boldsymbol{\varphi}(t)$, of dimension $N_s + 1$, is the composition vector consisting of species molar concentrations and temperature, and $\boldsymbol{k}$, of dimension d, is the vector of forward reaction rate constants of the d elementary reactions involved in a mechanism. See Appendix A for more details. Eq. (2) is integrated with a stiff ODE solver in Cantera

[18] with a given chemical mechanism. The IDT, τ, is defined as the time instance when the temperature gradient reaches maximum. With a given distribution for the rate constants $\boldsymbol{k}$, the PDF distribution of the QoI can be obtained and it is very often characterized by the mean value and its uncertainty, i.e., root mean square value.

Uncertainties in Arrhenius parameters A, b and E_a are systematically studied in [19,20] and the uncertainties of rate coefficient $\boldsymbol{k}$ from the pre-exponential factor and activation energy are in the same order and correlate well to each other. Thus, in this study only the uncertainty in A factor is considered and modeled by the uncertainty factor UF for the demonstration of uncertainty propagation in mechanism reduction. Furthermore, the method developed can be applied to the uncertainties in temperature exponent and activation energy if needed.

Following [6,21], the rate constants in this study are assumed to be independent log-normal distributions. Once centered and normalized as x_i, they follow the standard normal distributions,

$$\boldsymbol{x_i} = \frac{\ln \boldsymbol{k_i}/\boldsymbol{k_{i0}}}{\frac{1}{3}\ln \mathrm{UF}_{\boldsymbol{i}}} \sim \boldsymbol{N}(0,\ 1),\ \ \boldsymbol{i} = 1, \ldots, \boldsymbol{d} \tag{3}$$

where k_i is the ith reaction rate coefficient, k_{i0} and UF_i are its nominal value and uncertainty factor, d is the number of elementary reactions and is also the dimension of the original input parameter space. The simulation inputs are then represented as a d-dimensional random vector $\boldsymbol{x} = [x_1, \ \ldots, \ x_d]^T$. Denote the distribution of $\boldsymbol{x}$ as $\pi_{\boldsymbol{x}}$, which follows the multi-dimensional normal distribution. The deterministic forward combustion model maps the input parameters to the QoIs, and the map to a specific QoI is denoted as a function $f(\boldsymbol{x})$. For the autoignition study, the forward combustion model is Eq. (2) and the QoI is the IDT.

In general, uncertainty of the QoI can be quantified by Monte Carlo (MC) methods, where each sample in the parameter space corresponds to a response in QoI. With sufficient samples, the distribution of $f(\boldsymbol{x})$ can be obtained. However, due to the slow convergence of the MC method, a large number of samples are often required, particularly when the number of kinetic parameters is large.

2.3. Kinetic parameter reduction via active subspace method

Various response surface techniques have been adopted in conjunction with MC, in which one uses a few carefully selected runs of the expensive model to construct a cheaper response surface that is subsequently sampled for MC. However, building response surfaces requires a large number of runs of the expensive model when the number of input parameters is large. In this study, an integrated use of sensitivity analysis and active subspace (AS) [22,23] is proposed for the kinetic parameter reduction, in which sensitivity analysis is first employed to identify the important reactions and construct the reduced parameter subspace, and AS is then used to identify the important directions in the reduced subspace. Note that unlike sensitivity analysis that identifies the important individual input parameters, the AS approach identifies the important directions, i.e., linear combinations in the input parameter space, and can lead to further dimension reduction and requires much fewer runs of the expensive model.

For sensitivity analysis, the sensitivity of IDT, $S_{\tau,i} = \frac{k_i}{\tau}\frac{\partial \tau}{\partial k_i}$, is obtained with the brute-force finite difference approach. The accuracy of the sensitivity vector can be validated against those obtained from analytical adjoint method by inner product of the two vectors [24]. A subset of important reactions is then obtained according to the sensitivity magnitudes of individual reactions. The elimination of unimportant reactions will incur truncation error in the sensitivity vector, which is defined as

$$\epsilon_{\boldsymbol{S}} = 1 - \boldsymbol{S_{imp}^T S_{full}} \tag{4}$$

where $\boldsymbol{S}_{full}$ is the full sensitivity vector and $\boldsymbol{S}_{imp}$ only consists of the components corresponding to the important reactions. In this study, for a given mechanism, a minimum set of most sensitive reactions are first obtained for each thermochemical condition, which maintains the magnitude of the selected sensitivity vector being no smaller than 99% of that for the full one. The final set of important reactions for a given mechanism is the union of all the sensitive reactions for itself and its derived skeletal mechanisms under all thermochemical conditions. Therefore, the important reactions identified have accounted for the wide range of thermochemical conditions. At the meantime the truncation error ϵ_S is kept smaller than 1% for each mechanism under all tested thermochemical conditions. With sensitivity analysis, for the DME55 mechanism, only 32 out of the 290 reactions are identified as important (see Appendix B), which significantly reduces the cost for subsequent active subspace analysis.

2.3.1. Active subspace and Monte Carlo sampling

The active subspace method, as detailed in [22,25], seeks an r-dimensional subspace that describes most of the variation of function f. The idea is to find a low-dimensional approximation of f as

$$\boldsymbol{f}(\boldsymbol{x}) \approx \boldsymbol{\eta}(\boldsymbol{x_r}), \quad \boldsymbol{x_r} = \boldsymbol{S^T x}, \tag{5}$$

where η is a function of the r-dimensional input $\boldsymbol{x_r}$ with $r < d$, and $\boldsymbol{S}$ is a semi-orthogonal matrix of size $d \times r$. The active subspace is defined as span($\boldsymbol{S}$). One way to identify the active subspace is to perform an eigenvalue decomposition of the matrix $\boldsymbol{C}$, defined as the expectation of the outer product of the gradient ∇f with itself, i.e.,

$$\boldsymbol{C} = \int (\nabla \boldsymbol{f})(\nabla \boldsymbol{f})^{\boldsymbol{T}} \boldsymbol{\pi_x d x} = \boldsymbol{W \Lambda W^T} \tag{6}$$

Note that $\boldsymbol{C}$ is symmetric, positive semi-definite, and of size $d \times d$. The unitary matrix $\boldsymbol{W}$ consists of the d eigenvectors $\boldsymbol{w}_1, \ldots, \ \boldsymbol{w}_d$ and $\boldsymbol{\Lambda}$ is a diagonal matrix whose components are the eigenvalues $\lambda_1, \ \ldots, \ \lambda_d$, sorted in descending order. If there is a gap in the eigenvalues, meaning $\lambda_r \gg \lambda_{r+1}$, then the function f varies mostly along the first r eigenvectors. The first r eigenvectors are selected to span the active subspace $\boldsymbol{S} = [\boldsymbol{w}_1, \ \ldots, \ \boldsymbol{w}_r]$. The active subspace can be interpreted as the average gradient of the QoI over the uncertain parameter space. Then one can build a response surface, $\mathbf{RS}(\boldsymbol{x_r})$ with the active variables $\boldsymbol{x_r} = \boldsymbol{S^T x}$ as inputs. Denoting it by the function η, one has $f(\boldsymbol{x}) \approx \eta(\boldsymbol{x}_r) = \mathbf{RS}(\boldsymbol{x}_r)$. In practice, the integral of the gradients' outer product in the parameter space is obtained by Monte Carlo sampling with $M \approx d \times \ln d$ samples and the error in the estimated eigenvalues and eigenvectors due to insufficient number of runs can be estimated with bootstrapping method [22]. Various response surface techniques can be applied to the low-dimensional active subspace once it is identified. In this study, polynomial fitting is employed to construct the response surface of the IDTs.

2.4. Uncertainty analysis in mechanism reduction via transition state

2.4.1. Uncertainty quantification for individual mechanisms

In this study, the PCE method [6,21] is employed for the uncertainty quantification of individual mechanisms. PCE can explicitly yield the uncertainty of a polynomial equation with the probability distribution function (PDF) of inputs known as a prerequisite and, compared to MC, it does not incur any statistical error caused by sampling. Using PCE in conjunction with polynomial fitting for the response surface, a model prediction y as a function of $\boldsymbol{x_r}$ is expressed in terms of the Taylor series

$$\boldsymbol{y} = \boldsymbol{\eta}(\boldsymbol{x_r}) = \boldsymbol{y}_0 + \boldsymbol{g^T x_r} + \boldsymbol{x_r^T \mathbf{H} x_r} + \boldsymbol{h.o.t}, \tag{7}$$

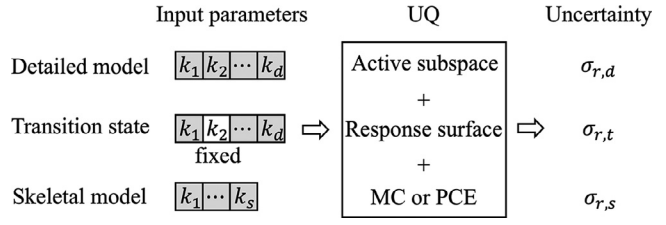

Fig. 1. Illustration of uncertainties for detailed model, transition state and skeletal model, where the one for transition state is obtained by fixing rate coefficients of eliminated reactions.

where $\mathbf{g} = \nabla y$ is the gradient of y, $\mathbf{H} = \frac{1}{2}\boldsymbol{J}(\nabla y)$ is the Hessian matrix, $\boldsymbol{J}$ is the Jacobian operator, and $h.o.t$ represents higher order terms. Noted that $\mathbf{g}$ and $\mathbf{H}$ in the polynomial expansion show the effects of first- and second-order sensitivities and can be obtained by sensitivity analysis, as detailed in [2]. In this work, the polynomial expansion $\eta(\boldsymbol{x_r})$ is trained by ordinary least square regression. For kinetic uncertainty, $x_i = \frac{\ln k_i/k_{i0}}{\frac{1}{3}\ln \mathrm{UF}_i} \sim N(0,\ 1)$ and the active subspace $\boldsymbol{S}$ is orthogonal, which indicates $\boldsymbol{x_r} = \boldsymbol{S}^T\boldsymbol{x}$ still follows multi-dimensional normal distribution. Thus, when $\boldsymbol{x_r} = 0$ (a null vector), $y = y_0$. The uncertainty of the response surface, i.e., σ_r, is related to the uncertainty in $\boldsymbol{x_r}$ and is given by

$$\boldsymbol{\sigma_r^2} = \mathbf{E}\left[\boldsymbol{yy}^T\right] - \mathbf{E}^2[\boldsymbol{y}] = \mathbf{g}^T\mathbf{g} + 2\boldsymbol{tr}(\mathbf{HH}) \tag{8}$$

where the first and second terms respectively represent the uncertainty from the first- and second-order parts of the response surface.

2.4.2. Uncertainty propagation in skeletal reduction: truncation and coupling

Assume that the number of elementary reactions has been reduced from d in the detailed mechanism to s in the skeletal mechanism. The input parameters of the detailed and skeletal mechanisms are $\boldsymbol{x}_d$ of dimension d, and $\boldsymbol{x}_s$ of dimension s, respectively, with each rate parameter following a standard normal distribution. In conjunction with the active subspace method, the uncertainty of response surfaces for the detailed and skeletal models can be written as

$$\sigma_{r,d} = \sigma\left[\eta_{r,d}\left(\boldsymbol{S}_d^T\boldsymbol{x}_d\right)\right] \tag{9}$$

$$\sigma_{r,s} = \sigma\left[\eta_{r,s}\left(\boldsymbol{S}_s^T\boldsymbol{x}_s\right)\right] \tag{10}$$

where $\boldsymbol{S}_d$ and $\boldsymbol{S}_s$ span the active subspaces of the detailed and skeletal mechanisms, respectively.

The uncertainty propagation during mechanism reduction is attributed to parameter truncation and reaction coupling. To decouple these two effects, as illustrated in Fig. 1, a transition state is defined such that the input parameter $\boldsymbol{x_t}$ is still d-dimensional, but only the rate parameters of the retained reactions follows the same normal distributions as the ones in the detailed mechanism. The rate parameters of the eliminated reactions are kept as nominal values for eliminating uncertainty. Then the input parameter for the transition state is given by $\boldsymbol{x_t} = \boldsymbol{P}\boldsymbol{x_d}$, where the components of the $d \times d$ diagonal transformation matrix $\boldsymbol{P}$ is one for the corresponding retained reactions and zero for the eliminated reactions. The uncertainty in the transition state is denoted as $\sigma_{r,\ t}$, which is obtained with $\boldsymbol{x_t}$ as the response surface input for the autoignition model with the detailed mechanism. The uncertainty change from the detailed mechanism to the transition state is therefore due to the truncation of uncertainty for the eliminated reactions.

With the truncated active subspace being defined as $\boldsymbol{PS_d}$, the uncertainty of the transition state can be represented as

$$\boldsymbol{\sigma_{r,t}} = \boldsymbol{\sigma}\left[\boldsymbol{\eta_{r,d}}\left(\left(\boldsymbol{PS_d}\right)^T\left(\boldsymbol{Px_d}\right)\right)\right]. \tag{11}$$

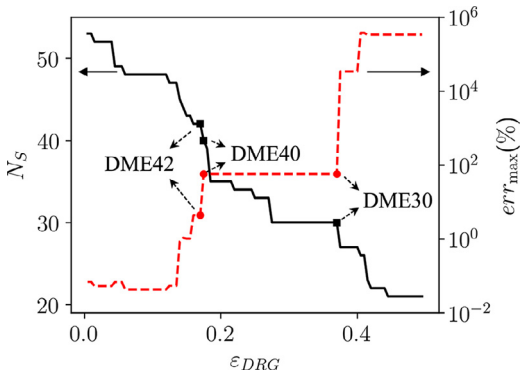

Fig. 2. The dependence of the number of retained species N_s and the maximum incurred error in IDTs on the reduction threshold ε_{DRG}. Also marked are the three representative mechanisms for uncertainty analysis.

With the transition state, the uncertainty change due to reaction coupling, i.e., the effect of the eliminated species/reactions on the retained species and reactions, can be straightforwardly obtained as $\sigma_{r,t} - \sigma_{r,s}$. The relative influence of parameter truncation and reaction coupling can be measured by the ratio

$$\boldsymbol{r_t} = \frac{\|\boldsymbol{\sigma_{r,d}} - \boldsymbol{\sigma_{r,t}}\|}{\|\boldsymbol{\sigma_{r,d}} - \boldsymbol{\sigma_{r,t}}\| + \|\boldsymbol{\sigma_{r,t}} - \boldsymbol{\sigma_{r,s}}\|} \tag{12}$$

A large r_t means that the uncertainty change mainly arises from uncertainty parameter truncation, otherwise reaction coupling is dominant for uncertainty change during the reduction process.

3. Results

Skeletal mechanisms of different sizes have been obtained using DRG implemented in PyMars [26-28], covering initial temperature of 650 $K \le T_0 \le$ 1200 K, pressure of 1 atm $\le P \le$ 20 atm, and equivalence ratio of $0.5 \le \phi \le 1.5$. The starting species for DRG are the fuel species CH_3OCH_3 and the oxidizer species O_2. The inert species N_2 is also retained in the skeletal mechanisms. At each threshold, a subset of reactions will be eliminated and the remained reactions constitute an intermediate skeletal mechanism. The maximum error of the QoI between the skeletal mechanism and detailed mechanism under all reference thermochemical conditions is denoted as $err_{\max}$.

Figure 2 shows the dependence of the number of retained species N_s on the reduction threshold ε_{DRG}, together with the maximum incurred error $err_{\max}$ in IDTs from the corresponding mechanisms. Note that with about ten species eliminated, the maximum error reaches up to 1%, which implies DME55 is a relative compact mechanism and contains few non-essential species. The jumps in the number of species at certain thresholds are due to the elimination of strong coupled species, thus the threshold for a skeletal mechanism is often selected either before or after such jumps, as detailed in [9].

As shown in Fig. 2, three representative skeletal mechanisms along the curve of maximum error are chosen for the analysis of their uncertainty propagation. The information is summarized in Table 1 with the eliminated species from the preceding mechanism being listed. Note that significant increase in the error for IDTs has been observed when species C_2H_5 and C_2H_6 are further removed from DME42 and N_s is reduced from 42 to 40 in DME40. In contrast, no noticeable increase in the maximum error is observed when ten additional species: CH_2, $CH_2(S)$, C_2H_2, C_2H_3, C_2H_4, HCCO, OCHO, CH_3OCHO, CH_3OCH_2O, $CH_3OCH_2O_2H$, are removed from DME40 and the number of species is reduced from 40 down to 30 in DME30.

Table 1
Three representative skeletal mechanisms obtained by DRG.

	N_S	N_R	err_{max}	Species eliminated from the preceding one
DME42	42	208	4.4%	C_2H, CH_2CO, $HCCOH$, CH_2HCO, CH_3CO, CH_3CHOH, C_2H_4OH, CH_3CH_2O, C_2H_5OH, CH_3OCH_2OH, $HOC_2H_4O_2$, AR, HE
DME40	40	192	56.8%	C_2H_5, C_2H_6
DME30	30	123	56.8%	CH_2, $CH_2(S)$, C_2H_2, C_2H_3, C_2H_4, HCCO, OCHO, CH_3OCHO, CH_3OCH_2O, $CH_3OCH_2O_2H$

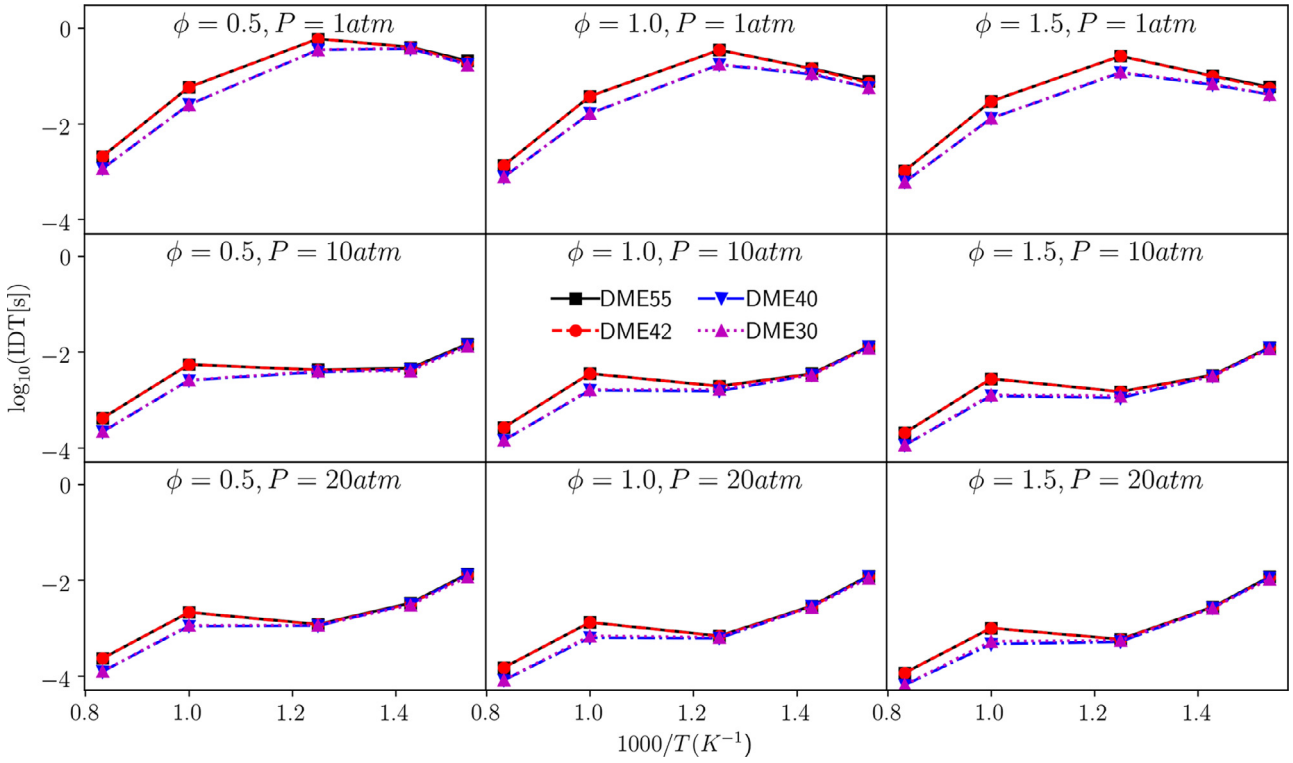

Fig. 3. The dependence of IDTs on initial temperature, equivalence ratio and pressure of DME/air mixtures.

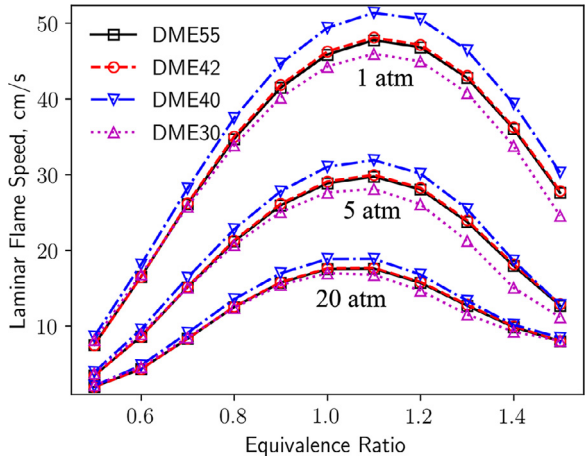

Fig. 4. Laminar flame speeds of premixed DME/air mixtures calculated with the detailed and skeletal mechanisms. The temperature of unburnt mixtures is 300 K.

Figure 3 demonstrates the accuracy of the skeletal mechanisms by showing the computed IDTs. As shown, significant errors are observed in general for the autoignition process under relatively high initial temperatures when reducing DME42 further down to DME40. The skeletal mechanisms are also validated against the detailed one by comparing the computed laminar flame speeds, which are not included in QoIs during reduction. Figure 4 shows the computed laminar speeds over a wide range of pressures and equivalence ratios for the unburned DME/air mixtures of 300 K. The computed flame speeds from DME42 agree well with those from DME55, but noticeable differences between DME 40, DME30 and DME55 are observed, particularly under low-pressure and fuel-rich conditions. Nevertheless, even only IDTs are considered as QoIs during the reduction processes, the incurred relative errors in laminar flame speeds are less than 10% for all the tests shown in Fig. 4. The observations are consistent with the ones in Ref [2]. Hence only IDTs being selected as target for reduction is sufficient for current study.

To further examine the difference among the mechanisms, Figure 5 shows the computed temperature profiles for representative one-stage and two-stage DME-air auto-ignition process, under two representative conditions. As shown in Fig. 5a, the reduction from DME42 to DME40 yields significant error in the prediction for high-temperature auto-ignition, which indicates that the species C_2H_5 along with C_2H_6 and related reactions are crucial for high-temperature chemistry. The eliminated reactions from DME42 to DME40 are listed in Table 2 and show that the methyl radical branching reaction R52, which is important in high-temperature chemistry, is removed. And most of C_2H_5-containing reactions in Table 2 are related to C_2H_6. Once C_2H_6 is removed, C_2H_5 that strongly coupled with C_2H_6 will be removed automatically. In contrast, as shown in Fig. 5b, the reductions from DME55 to DME42 and from DME40 to DME30 lead to noticeable error in the first-stage ignition process, implying that the removed species and reactions have influential effects on low-temperature chem-

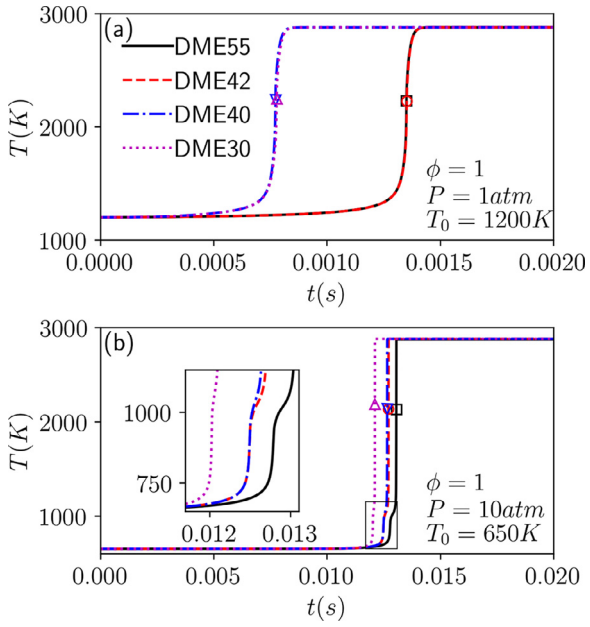

Fig. 5. The temperature profiles from stoichiometric DME-air auto-ignition with different mechanisms. Symbols represent the ignition point. (a) is under $P = 1$atm and $T_0 = 1200$K, of which the high-temperature pathway is dominant, and (b) is low-temperature pathway controlled with $P = 10$atm and $T_0 = 650$K.

Table 2
The eliminated reactions from DME42 to DME40.

Index	Reaction
R52	$2CH_3$ (+M) [=] C_2H_6 (+M)
R94	$2CH_3$ [=] C_2H_5 + H
R103	C_2H_6 + H [=] C_2H_5 + H_2
R104	C_2H_6 + O [=] C_2H_5 + OH
R105	C_2H_6 + OH [=] C_2H_5 + H_2O
R106	C_2H_6 + O_2 [=] C_2H_5 + HO_2
R107	C_2H_6 + HO_2 [=] C_2H_5 + H_2O_2
R108	C_2H_6 + CH_3 [=] C_2H_5 + CH_4
R109	C_2H_5 + H (+M) [=] C_2H_6 (+M)
R110	C_2H_5 + H [=] C_2H_4 + H_2
R111	C_2H_5 + O [=] CH_2O + CH_3
R112	C_2H_5 + O_2 [=] C_2H_4 + HO_2
R113	$2C_2H_5$ [=] C_2H_4 + C_2H_6
R114	C_2H_5 + HCO [=] C_2H_6 + CO
R115	C_2H_5 + O [=] CH_3HCO + H
R117	C_2H_4 + H (+M) [=] C_2H_5 (+M)

istry pathway. Recalling that the main focus of this study is to investigate the uncertainty propagation in skeletal reduction using representative mechanisms, instead of developing accurate skeletal mechanisms for combustion simulations. Thus, the three skeletal mechanisms, with noticeable errors either in high-temperature pathway or low temperature pathway, are generated and used to demonstrate the uncertainty analysis.

3.1. Dimension reduction of kinetic parameters

Over the range of equivalence ratio, pressure and initial temperature considered, for the DME55 mechanism, with sensitivity analysis, only 32 of the 290 reactions are identified as important and the corresponding kinetic parameters are identified important (See Appendix A for the list of all the important reactions). The important reactions are compared and examined with previous sensitivity analysis in [29–32], and good consistence in the key reactions

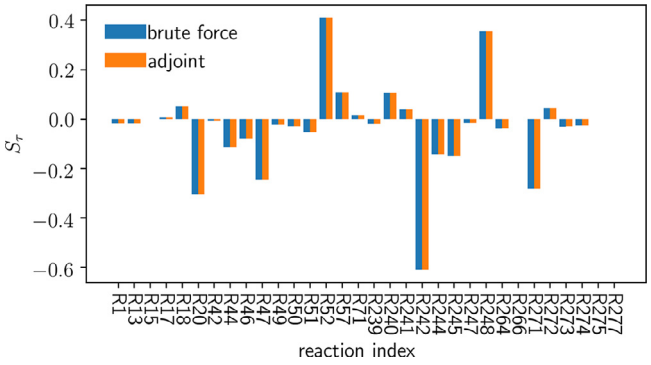

Fig. 6. The sensitivities of IDTs from the brutal force and the adjoint methods for DME55 under $\{\phi,\ P,\ T_0\} = \{1.0, 1\text{atm}, 1000\text{K}\}$. The perturbation factor is 5×10^{-3} for the brutal force method.

are obtained. Note that R52 is related to C_2H_6 and no reaction related to C_2H_5 is identified to be important, which is consistent with the analysis in the reduction process from DME42 to DME40.

The accuracy of sensitivity vectors obtained with finite difference is validated with those from the adjoint method. As shown in Fig. 6, the inner product of the two unit sensitivity vectors is no smaller than 0.99 for almost all the tests considered. This verifies the accuracy in the finite difference approach for computing sensitivity vectors.

Considering that the sensitivity vector may vary with different kinetic parameters, further analysis is performed for more random samples in the uncertainty space. It confirms that the 32 selected parameters maintain important and sufficient, since for almost all samples the length of sensitivity vector in the 32 dimensions is larger than 99% of the full sensitivity vector. In the following, the active subspace is constructed within the parameter space only for the important reactions identified by sensitivity analysis.

With the identified 32 important kinetic parameters, for each thermochemical condition $\{\phi, P, T_0\}$, the analysis of active subspace has been performed. The uncertainty factors UF = 5 are employed for all the kinetic parameters for demonstration. Note that if the uncertainties for certain reactions have been well investigated and have more appropriate uncertainty factors, one can directly incorporate this information without any difficulty. For the autoignition of stoichiometric DME/air mixture with $P = 10$atm and $T_0 = 1000K$, the corresponding eigenvalues of matrix C estimated using $M = 400$ samples are shown in Fig. 7a. It is seen that the first eigenvalue is much larger than the second one, implying the existence of a one-dimensional active subspace. This is further confirmed by the summary plot of Fig. 7b, which shows the distribution of IDTs along the first active variable, *i.e.*,$\boldsymbol{w}_1^T\boldsymbol{x}$. The IDTs lie close to a one-dimensional curve and the scattering in the direction orthogonal to the active direction is small. The components of the active direction, i.e., the first eigenvector, are shown in Fig. 7c. The corresponding values are plotted against the original reaction index instead of the order in the 32 important reactions. The most sensitive reactions are three CH_3-related reactions, i.e., $2CH_3$ (+M) = C_2H_6 + M (R52), CH_3OCH_2 = CH_2O + CH_3 (R248) and CH_3 + CH_3OCH_3 = CH_3OCH_2 + CH_4 (R242). Note that the largest positive value in R52 corresponds to the recombination of methyl radical, which is consistent with the major importance of methyl radical branching reactions in the DME kinetics [26,27]. Thus, the removal of C_2H_6 and C_2H_5 in DME40 results in significant error. In addition, R242 is the most important H-abstraction reaction, and R248 is an important β-scission process to form formaldehyde and the methyl radical.

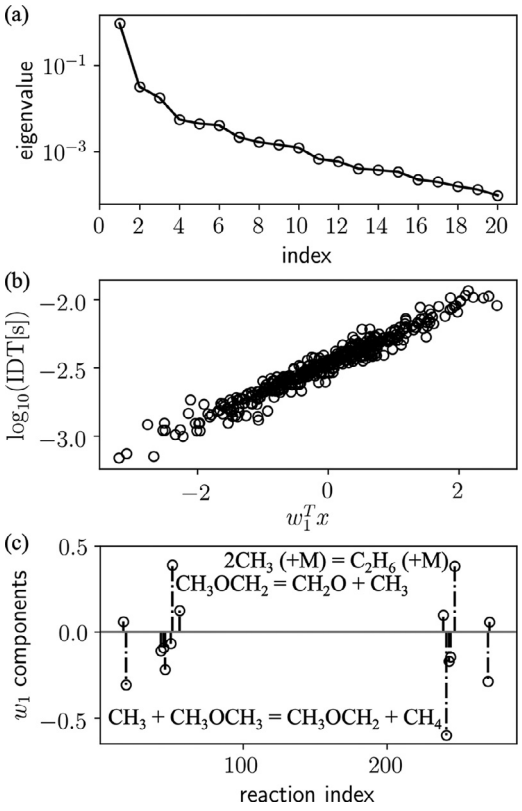

Fig. 7. (a) The eigenvalues of the corresponding matrix C; (b) the summary plot of the IDT being plotted against the active variable; (c) the individual component (with magnitude being greater than 0.05) of the first active direction.

3.2. Uncertainty propagation in mechanism reduction

For conservative consideration, the first three active directions are chosen to span the active subspace. Then a three-dimensional response surface based on second-order polynomial fitting is built for individual mechanisms under each thermochemical condition $\{\phi, P, T_0\}$. With half of the data for training and the other half for validation, the accuracy of response surface is validated as shown in Fig. 8a, with the prediction of response surface versus the real data lies close to the linear relationship line. Figure 8b shows the distribution of IDTs along with $\boldsymbol{w}_1^T\boldsymbol{x}$, in which the black dots are 50,000 samples for the MC method to obtain the statistics of IDTs. Note that all samples lie close to the one-dimensional curve of training data, which substantiates the accuracy and effectiveness of the response surface. The PDF of IDTs are shown in Fig. 8c. There is good agreement between PDFs of the training data and the predictions, which demonstrates the sufficient accuracy of the three-dimensional active subspace in propagating the kinetic uncertainty. To further confirm the accuracy of active subspace and response surface method, 10,000 individual Monte Carlo samples in the kinetic parameter space are solved by Cantera and then compared with Monte Carlo samples propagated by response surface. As shown in Fig. 8d, the relative error for the uncertainty σ is smaller than 1%, and the relative error for the mean value is smaller than 0.1%.

Note that the active subspace is constructed within the parameter space only for the important reactions identified by sensitivity analysis. The threshold value for keeping important reactions after sensitivity index may have impact on the active subspace and subsequent analysis. Here the dependence of uncertainty analysis on the truncation error of the sensitivity vector is investigated. To achieve so, sensitivity analyses $S_{\tau,i} = \frac{k_i}{\tau}\frac{\partial \tau}{\partial k_i}$ are first performed

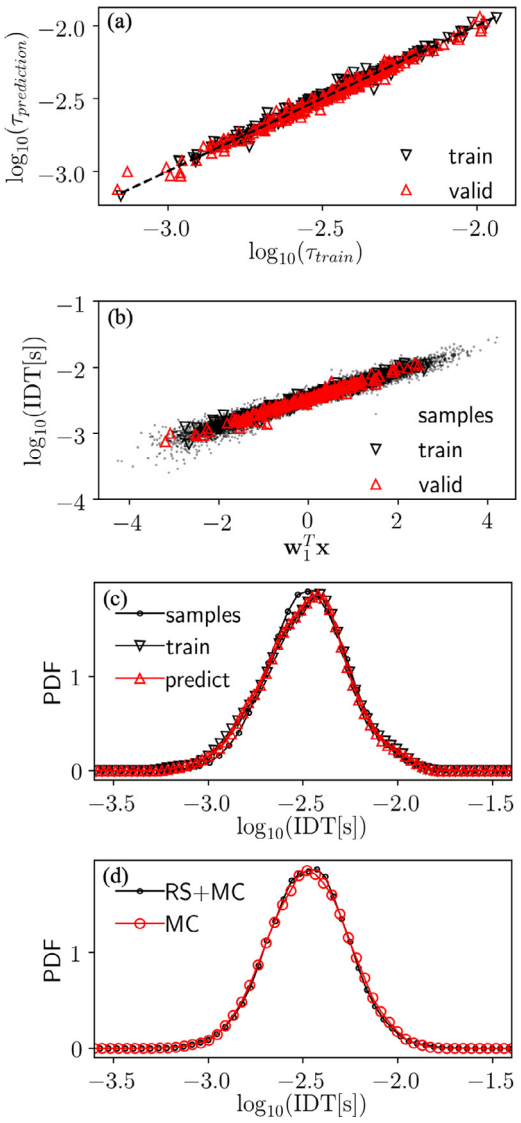

Fig. 8. The training and validation progress, (a) the training and validation; (b) the $\boldsymbol{w}_1$ projection of 50,000 samples of response surface; (c) PDF plot of samples, under $\{\phi, \mathrm{P}, \boldsymbol{T}_0\} = \{1.0,\ 10\mathbf{atm},\ 1000\boldsymbol{K}\}$; (d) comparison between PDF plots of MC samples propagated by response surface and MC samples integrated by an ODE solver.

at nominal parameters for all the thermochemical conditions considered, and reactions are then sorted by their corresponding sensitivities in magnitude, i.e., sensitivity index. Then the dependence analysis can be performed for individual thermochemical condition.

For demonstration, Fig. 9a shows the incurred errors in the active direction w_1, the mean μ_r and r.m.s σ_r of $\log_{10}$(IDT) against the truncation error in sensitivity vector for the condition of ϕ =1, P = 1atm and T_0 = 1200K. This is obtained by first simulating 6400 independent random auto-ignition samples in kinetic parameter space with full sensitivities under this particular thermochemical condition. A series of sensitivity vectors are then obtained by sequentially removing the unimportant reactions according to their sensitivity indexes. For each individual sensitivity vector, the truncation error ϵ_S can be computed accordingly with Eq. (4). And the active subspace and response surface can be built with 400 random samples. The errors in the first active direction w_1, mean value μ_r and r.m.s σ_r of the response surface can be obtained by comparing against those built from all 6400 samples with full

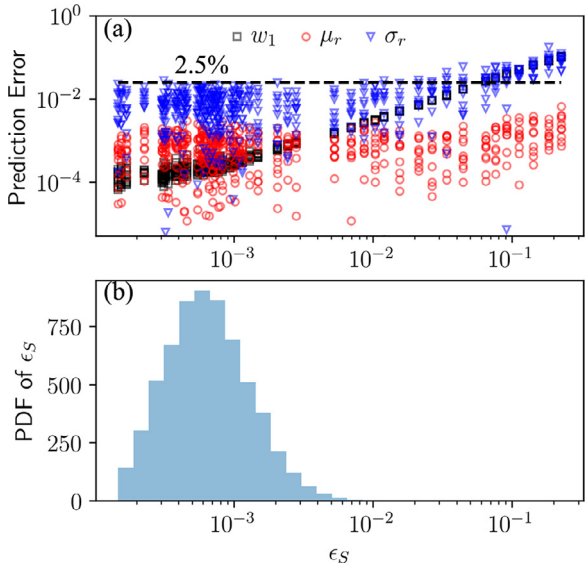

Fig. 9. (a) The incurred errors in the active direction w_1 (black square), the mean μ_r (red circle) and r.m.s σ_r (blue triangle) of $\log_{10}$(IDT), against the truncation error ϵ_S in sensitivities, (b) the PDF distribution of the sensitivity truncation errors in kinetic parameter space, under the condition of ϕ =1, P = 1atm and $T_0 = 1200K$. (For interpretation of the references to color in this figure legend, the reader is referred to the web version of this article.)

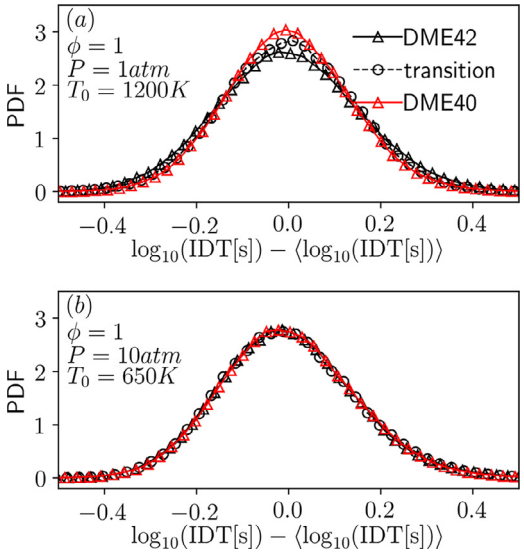

Fig. 10. The evolution of PDFs for IDTs (centering around the mean values) during the reduction from DME42 to DME40. For high-temperature pathway in (a), the uncertainty decrease from detailed model $\sigma_{r,d} = 0.1534$ to transition state $\sigma_{r,t} = 0.1422$ and to skeletal model $\sigma_{r,s} = 0.1343$; and for low-temperature pathway in (b), the uncertainty change is insignificant with $\sigma_{r,d} = 0.1473$, $\sigma_{r,t} = 0.1478$ and $\sigma_{r,s} = 0.1454$.

sensitivity vector. For each sensitivity vector, the validation process is repeated ten times independently to avoid the potential bias from random samples. It is clear from Fig. 9a that the error in w_1 correlate well with the truncation error ϵ_S and it can be neglected when truncation error is smaller than 1%. The predicted mean value μ_r with 400 samples is generally accurate with errors being smaller than 0.1% for almost all tests. The error in σ_r comes from two contributions. As shown in Fig. 9a, when the sensitivity vector is sufficiently accurate (i.e., with ϵ_S being less than 5%), the error in σ_r results from a finite number of Monte Carlo samples for constructing response surface and it is confirmed to be less than 2.5% (as indicated by the black dashed line). Noted that the mean prediction error of σ_r is around 1%, among repeated sampling tests in the parameter space. When the sensitivity truncation error is

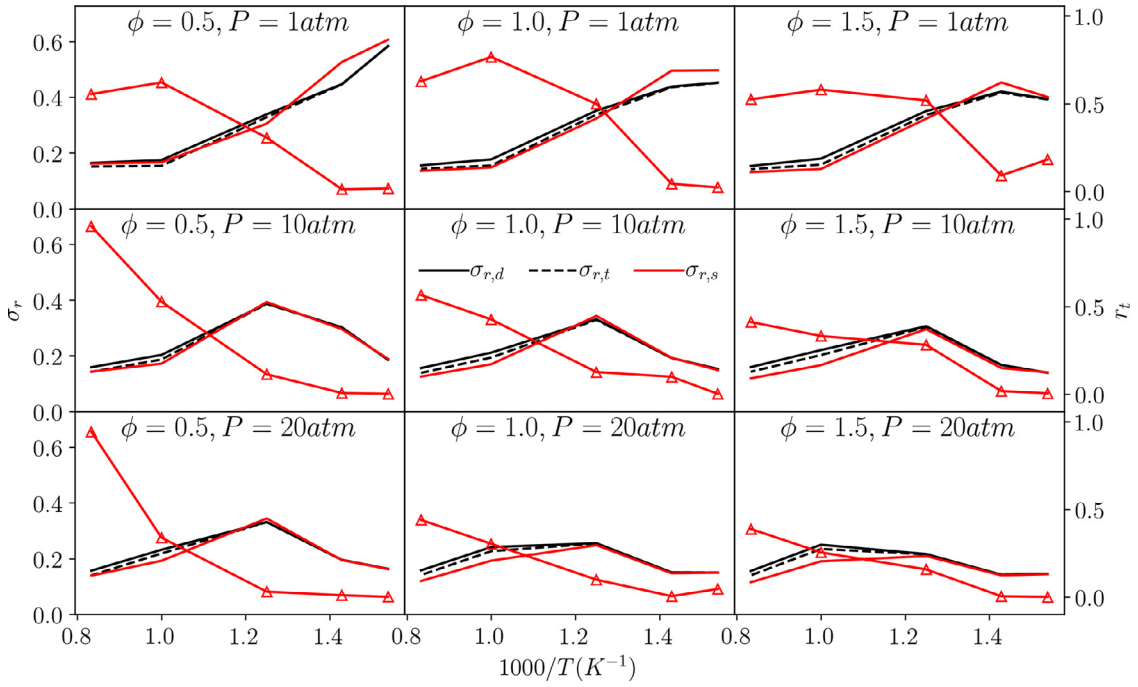

Fig. 11. Uncertainties in IDTs (in log10) for DME42, DME40 and the transition state from DME42 to DME40, for DME-air autoignition. $\sigma_{r,d}$ (black line), $\sigma_{r,t}$ (black dashed line), $\sigma_{r,s}$ (red line) represent the uncertainties in IDTs for DME42, transition state from DME42 to DME40, and DME 40, respectively, under each thermochemical condition. r_t (the red line with symbol) represents the relative contribution of parameter truncation for uncertainty change. (For interpretation of the references to color in this figure legend, the reader is referred to the web version of this article.)

significant, the error in σ_r will grow with the sensitivity error, and moreover grow in line with the error in active subspace.

Figure 9b shows the PDF of the sensitivity truncation errors of random samples in the parameter space. It shows the maximum error is less than 1% and this will incur less than 2.5% error in uncertainty analysis as shown in Fig. 9a. This confirms that the first layer of parameter reduction by sensitivity analysis in this study is adequate. Similar observations are made for other conditions.

Figure 10 shows the evolution of the PDFs of IDTs during the reduction from DME42 to DME40, which are obtained by 50,000 Monte Carlo samples in the kinetic parameter spaces. As shown in Fig. 10a, the uncertainty decreases as implied by the narrower PDFs for the autoignition process at high temperature, $T_0 = 1200K$. And both the truncation and reaction coupling contribute to the uncertainty reduction as implied by the PDF of the transition state staying in between. In contrast, for the autoignition process at low temperature, $T_0 = 650K$, the uncertainty in IDTs remains almost unchanged since the three PDFs remain the same, in Fig. 10b.

With the uncertainties of the mechanisms and the corresponding transition state being computed by solving the expectation of response surface in Eq. (8), the effects of parameter truncation and reaction coupling on uncertainty propagation are further quantified. Figure 11 shows the uncertainty propagation in the reduction from DME42 to DME40. Recall that species C_2H_5 and C_2H_6 are removed during the reduction, which results in significant error in the IDTs for high temperature autoignition (see Fig. 3). Under each individual pressure, the relative contribution of reaction coupling on uncertainty propagation decreases with temperature. For high temperature ignition, e.g., $T_0 > 800K$, with pressure increases from 1atm to 20atm, reaction coupling becomes more important for uncertainty change, as implied by the observation that the uncertainty curve for the transition state gradually approaches toward the one for DME42. Also shown is the evolution of $r_t = \frac{\|\sigma_{r,d} - \sigma_{r,t}\|}{\|\sigma_{r,d} - \sigma_{r,t}\| + \|\sigma_{r,t} - \sigma_{r,s}\|}$, representing the contribution of parameter truncation on uncertainty propagation. Parameter truncation in general has significant impact for high-temperature ignition of DME/air mixtures under relatively low pressures. Similar observations are made for each equivalence ratio during the reduction from DME42 to DME40. The uncertainty propagation in the reduction from DME55 to DME42 and from DME40 to DME30 are also analyzed and shown in Appendix B. The uncertainty changes in the two propagations are slightly relevant, which means that these reductions do not lead to significant change in both the mean and the uncertainty of IDTs, under selected thermochemical conditions.

Since the truncation in the first active direction $Pw_{d,1}$ has the largest influence on the uncertainty change, the uncertainty of detailed model and transition state can be approximated by:

$$\sigma_{r,d} = \sigma\left[\eta_{r,d}\left(S_d^T x_d\right)\right] \approx \sigma\left[\eta_{r,d}\left(w_{d,1}^T x_d\right)\right], \tag{13}$$

$$\sigma_{r,t} = \sigma\left[\eta_{r,d}\left((PS_d)^T (Px_d)\ \right)\right] \approx \sigma\left[\eta_{r,d}\left(\left(Pw_{d,1}\right)^T x_d\ \right)\right]. \tag{14}$$

With the mapping from kinetic parameters to the QoI being almost linear as shown in Fig. 7(b), the uncertainty change from the detailed mechanism to the transition state can be approximated by $\sigma_{r,t}/\sigma_{r,d} \approx \|Pw_{d,1}\|/\|w_{d,1}\| = \|Pw_{d,1}\|$. This has been confirmed in Fig. 12. The uncertainty change resulting from the uncertainty parameter truncation is almost linear with the change in the most active direction. Thus, the transition state analysis can be performed by considering only the truncation in active subspace, which can further reduce the computational cost.

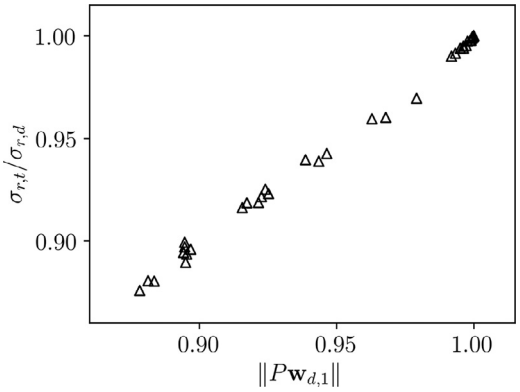

Fig. 12. The linear correlation between uncertainty change $\sigma_{r,t}/\sigma_{r,d}$ with the change in the most active direction $\|\boldsymbol{Pw}_{\boldsymbol{d},1}\|$.

4. Conclusions

Efficient and quantitative uncertainty analysis in mechanism reduction via the methods of active subspace and transition state analysis has been formulated and demonstrated in the reduction process of a 55-species, 290-reaction DME mechanism. Results show that sensitivity analysis can reduce the number of kinetic parameters from 290 down to 32 and an active subspace of very few dimensions e.g., 1–3 can be further identified within this 32-dimensional subspace for constructing the response surface of the IDTs. The cost for constructing a second order polynomial response surface is proportional to the square of input parameter dimension size. Consequently, uncertainty quantification can be performed with samples that are at least two orders of magnitude less.

With the PCE method being employed for the uncertainty quantification of individual mechanisms, the proposed transition state analysis decouples and quantifies the uncertainty change arising from uncertainty parameter truncation and reaction coupling during reduction. For the three representative skeletal mechanisms, the reduction process from DME42 to DME40 has influential effect on high-temperature reaction pathway, and the other two reduction processes, i.e., from DME55 to DME42 and from DME40 to DME30, mainly affects the low-temperature pathway. The reaction coupling effect is found to be significant for uncertainty changes at low temperature regime, in general, while parameter truncation is dominant at high temperatures. In addition, the uncertainty change associated with parameter truncation is proportional to the change in the most active direction.

Declaration of Competing Interest

The authors declare that they have no known competing financial interests or personal relationships that could have appeared to influence the work reported in this paper.

Acknowledgments

The work is supported by the National Natural Science Foundation of China No. 91841302, No. 52025062 and the National Science and Technology Major Project (2017-I-0004-0005).

Appendix A. Governing equations for the adiabatic, isochoric autoignition process

The governing equations for adiabatic, isochoric autoignition, a process widely applied in internal combustion engines, are

$$\frac{dc_i}{dt} = \nu_{ij}\omega_j \tag{R.1}$$

$$\frac{dT}{dt} = -(h_i - RT)\nu_{ij}\omega_j/\varsigma, \tag{R.2}$$

where c_i is the molar concentration of species i, T is mixture temperature, ν_{ij} is the stoichiometric coefficient of species i in reaction j, h_i is the total molar enthalpy of the ith species, ς is the molar weighted constant volume specific heat given by $\varsigma = c_i C_{v,i}$ with $C_{v,i}$ being the constant volume specific heat of species i, and ω_j is the net reaction rate of reaction j. Note that Einstein summation convention applies over the N_s species and d elementary reactions in the ideal gas mixture. The net reaction rate of reaction j is given by

$$\omega_j = k_{j,f}\left(\prod_{i=1}^{N_s} c_i^{\nu'_{ij}} - K_{c,j}^{-1}\prod_{i=1}^{N_s} c_i^{\nu''_{ij}}\right), \tag{R.3}$$

where ν'_{ij} and ν''_{ij} are the forward and reverse stoichiometric coefficients, respectively, and $K_{c,j}$ is the equilibrium constant of reaction j, $k_{j,f}$ is the forward rate constant given by the Arrhenius function

$$k_{j,f} = A_j T^{b_j}\exp\left(-\frac{E_{a,j}}{RT}\right), \tag{R.4}$$

where A_j is the pre-exponential factor, b_j is the temperature exponent, $E_{a,j}$ is the activation energy of the jth elementary reaction.

Let $\boldsymbol{\varphi}(t)$, of dimension $N_s + 1$, consist of the molar concentrations c_i and temperature T, the governing ODE could be written in the following compact form

$$\frac{d\boldsymbol{\varphi}}{dt} = \boldsymbol{F}(\boldsymbol{\varphi}; \boldsymbol{k}), \tag{R.5}$$

where $\boldsymbol{k}$, of dimension d, is the forward reaction rate constants of the d elementary reactions, i.e., $\boldsymbol{k} = [k_{1,f}, k_{1,f}, \ldots, k_{d,f}]$. In this study, the uncertainty in the jth elementary reaction is represented by the uncertainty of the rate constant $k_{j,f}$, which essentially represents the uncertainty lays in the pre-exponential factor A_j.

Appendix B. The list of important reactions identified by sensitivity analysis

Index	Reaction
R1	$H + O_2$ [=] $O + OH$
R13	$H + O_2$ (+M) [=] HO_2 (+M)
R15	$H + HO_2$ [=] $2OH$
R17	$HO_2 + OH$ [=] $H_2O + O_2$
R18	$2HO_2$ [=] $H_2O_2 + O_2$
R20	H_2O_2 (+M) [=] $2OH$ (+M)
R42	$CH_2O + H$ [=] $H_2 + HCO$
R44	$CH_2O + OH$ [=] $H_2O + HCO$
R46	$CH_2O + HO_2$ [=] $H_2O_2 + HCO$
R47	$CH_2O + CH_3$ [=] $CH_4 + HCO$
R49	$CH_3 + O_2$ [=] $CH_3O + O$
R50	$CH_3 + O_2$ [=] $CH_2O + OH$
R51	$CH_3 + HO_2$ [=] $CH_3O + OH$
R52	$2CH_3$ (+M) [=] C_2H_6 (+M)
R57	$CH_3 + HO_2$ [=] $CH_4 + O_2$
R71	$CH_3O + M$ [=] $CH_2O + H + M$
R239	CH_3OCH_3 [=] $CH_3 + CH_3O$
R240	$CH_3OCH_3 + OH$ [=] $CH_3OCH_2 + H_2O$
R241	$CH_3OCH_3 + H$ [=] $CH_3OCH_2 + H_2$
R242	$CH_3 + CH_3OCH_3$ [=] $CH_3OCH_2 + CH_4$
R244	$CH_3OCH_3 + HO_2$ [=] $CH_3OCH_2 + H_2O_2$
R245	$CH_3OCH_3 + O_2$ [=] $CH_3OCH_2 + HO_2$
R247	$CH_3OCH_2O_2 + CH_3OCH_3$ [=] $CH_3OCH_2 + CH_3OCH_2O_2H$
R248	CH_3OCH_2 [=] $CH_2O + CH_3$
R264	$CH_3OCH_2 + O_2$ [=] $CH_3OCH_2O_2$
R266	$2CH_3OCH_2O_2$ [=] $2CH_3OCH_2O + O_2$
R271	$CH_3OCH_2O_2$ [=] $CH_2OCH_2O_2H$
R272	$CH_2OCH_2O_2H$ [=] $2CH_2O + OH$
R273	$CH_2OCH_2O_2H + O_2$ [=] $O_2CH_2OCH_2O_2H$
R274	$O_2CH_2OCH_2O_2H$ [=] $HO_2CH_2OCHO + OH$
R275	HO_2CH_2OCHO [=] $OCH_2OCHO + OH$
R277	$HOCH_2OCO$ [=] $CO + HOCH_2O$

Appendix C. Uncertainty analysis of the other two reduction processes

The reduction processes from DME55 to DME42 and from DME40 to DME30 are also analysed. As shown in Fig. A1, the

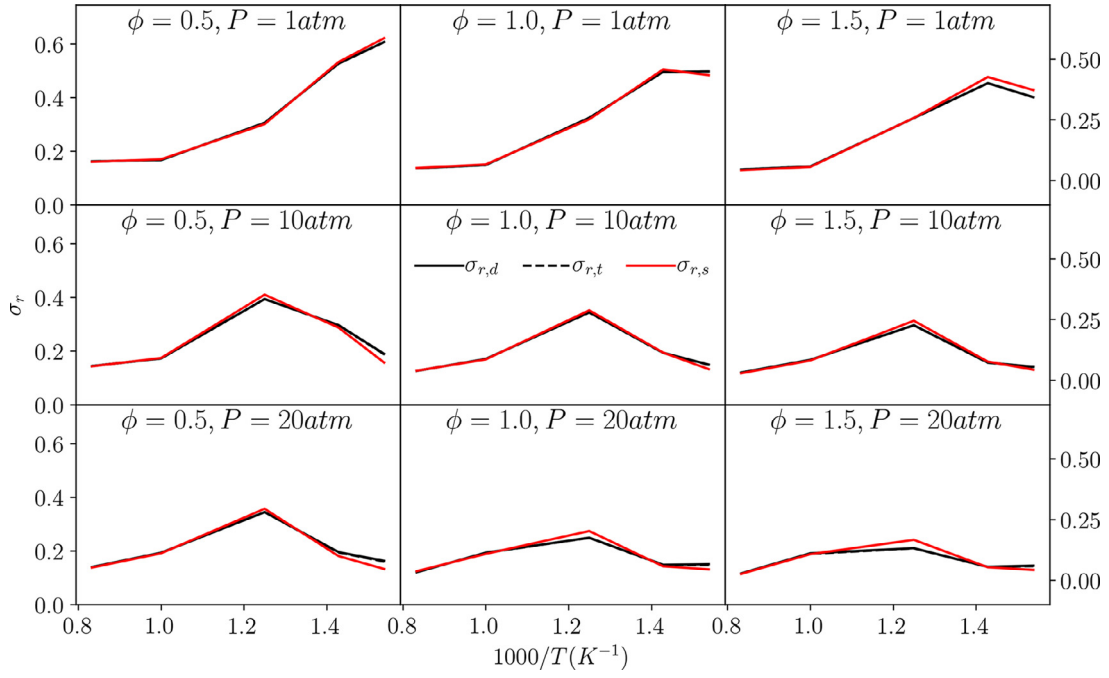

Fig. A1. Uncertainty in IDTs (in log10) for DME40, DME30 and the transition state from DME40 to DME30, for DME-air autoignition. Lines and dashed lines are uncertainty in IDTs under each thermochemical condition. Almost all the dashed lines overlap with the black lines, indicating that the effect of truncation in parameter space is weak.

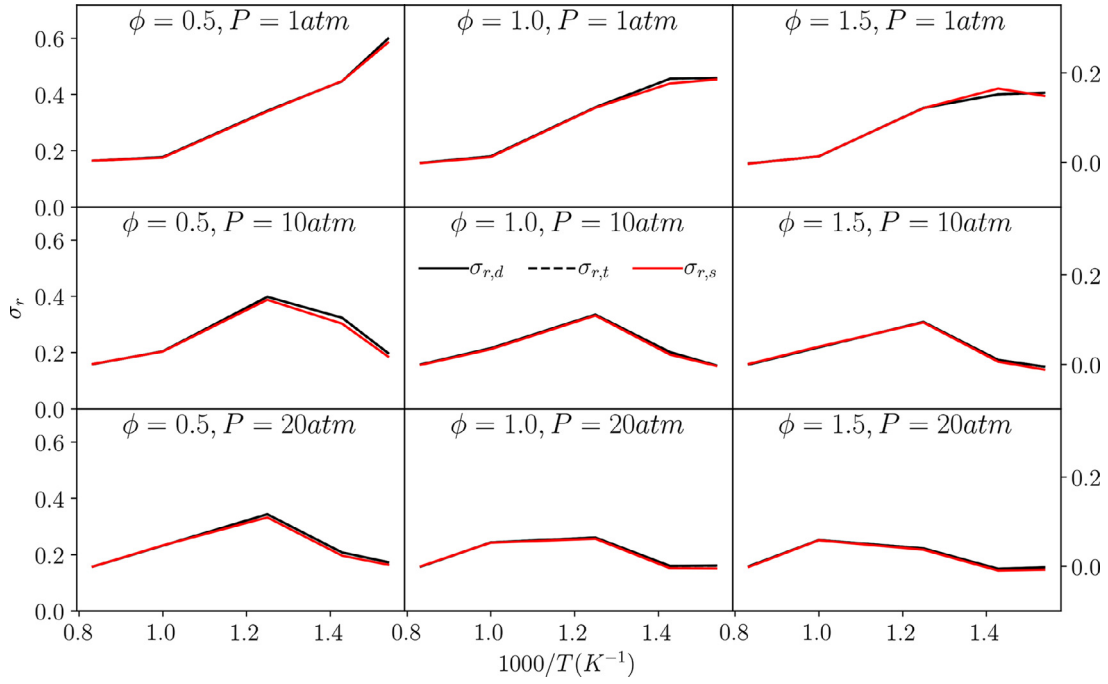

Fig. A2. Uncertainty in IDTs (in log10) for DME55, DME42 and the transition state from DME55 to DME42, for DME-air autoignition. Lines and dashed lines are uncertainties in IDTs under each thermochemical condition. Almost all the dashed lines overlap with the black lines, indicating that the effect of truncation in parameter space is weak.

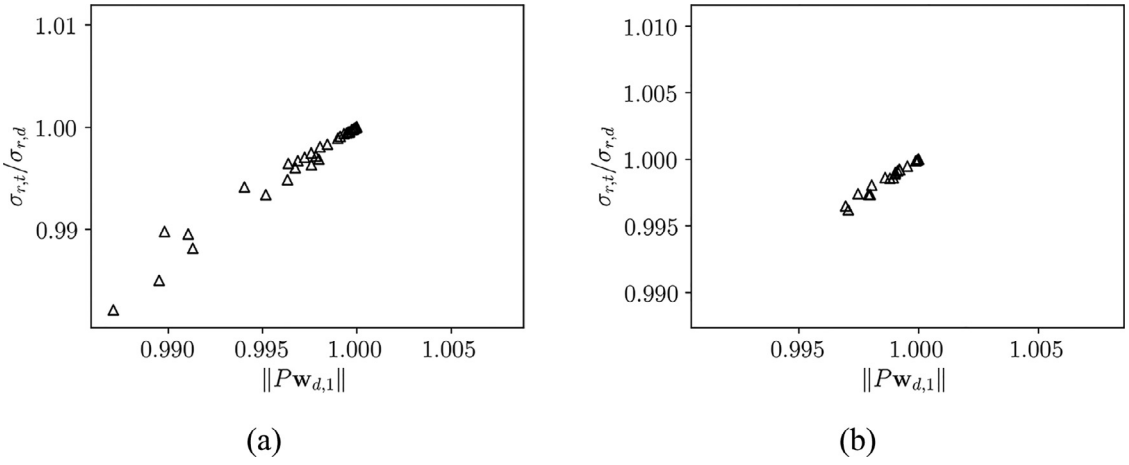

Fig. A3. The linear correlation between uncertainty change $\sigma_{r,t}/\sigma_{r,d}$ with the change in the most active direction $\|\boldsymbol{Pw_{d,1}}\|$, (a) the reduction from DME40 to DME30, (b) the reduction from DME55 to DME42.

reduction process from DME40 to DME30 shows no significant uncertainty change under most thermochemical conditions, especially at high temperature range. And the uncertainties of transition state overlap well with those of the detailed model DME40, which means that the truncation is weak during this reduction process. The results of the reduction process from DME55 to DME42 also show slightly uncertainty change only at low temperature and the truncation in uncertainty is negligible, as shown in Fig. A2.

In addition, the linear correlation between uncertainty change $\sigma_{r,t}/\sigma_{r,d}$ with the change in the most active direction $\|\boldsymbol{Pw_{d,1}}\|$ is confirmed in Fig. A3. The good linearity of the two reduction processes show consistence with the linear correlation approximation as stated in Section 3.2.

References

[1] T. Lu, C.K. Law, Toward accommodating realistic fuel chemistry in large-scale computations, Prog. Energy Combust. Sci. 35 (2009) 192–215.
[2] H. Wang, D.A. Sheen, Combustion kinetic model uncertainty quantification, propagation and minimization, Prog. Energy Combust. Sci. 47 (2015) 1–31.
[3] A.S. Tomlin, E. Agbro, V. Nevrlý, J. Dlabka, M. Vašinek, Evaluation of combustion mechanisms using global uncertainty and sensitivity analyses: a case study for low-temperature dimethyl ether oxidation, Int. J. Chem. Kinet. 46 (2014) 662–682.
[4] H. Rabitz, Ö.F. Aliş, J. Shorter, K. Shim, Efficient input—output model representations, Comput. Phys. Commun. 117 (1999) 11–20.
[5] H.N. Najm, B.J. Debusschere, Y.M. Marzouk, S. Widmer, O.P. Le Maître, Uncertainty quantification in chemical systems, Int. J. Numer. Methods Eng. 80 (2009) 789–814.
[6] D.A. Sheen, H. Wang, The method of uncertainty quantification and minimization using polynomial chaos expansions, Combust. Flame 158 (2011) 2358–2374.
[7] W. Ji, Z. Ren, Y. Marzouk, C.K. Law, Quantifying kinetic uncertainty in turbulent combustion simulations using active subspaces, Proc. Combust. Inst. 37 (2019) 2175–2182.
[8] Y. Xin, D.A. Sheen, H. Wang, C.K. Law, Skeletal reaction model generation, uncertainty quantification and minimization: combustion of butane, Combust. Flame 161 (2014) 3031–3039.
[9] T. Lu, C.K. Law, A directed relation graph method for mechanism reduction, Proc. Combust. Inst. 30 (2005) 1333–1341.

[10] S.H. Lam, D.A. Goussis, Understanding complex chemical kinetics with computational singular perturbation, Proc. Combust. Inst. 22 (1989) 931–941.
[11] T. Turányi, Applications of sensitivity analysis to combustion chemistry, Reliab. Eng. Syst. Saf. 57 (1997) 41–48.
[12] S. Vajda, P. Valko, T. Turányi, Principal component analysis of kinetic models, Int. J. Chem. Kinet. 17 (1985) 55–81.
[13] Z. Zhao, M. Chaos, A. Kazakov, F.L. Dryer, Thermal decomposition reaction and a comprehensive kinetic model of dimethyl ether, Int. J. Chem. Kinet. 40 (2008) 1–18.
[14] R.M. Galassi, M. Valorani, H.N. Najm, C. Safta, M. Khalil, P.P. Ciottoli, Chemical model reduction under uncertainty, Combust. Flame 179 (2017) 242–252.
[15] S. Deng, P. Zhao, D. Zhu, C.K. Law, NTC-affected ignition and low-temperature flames in nonpremixed DME/air counterflow, Combust. Flame 161 (2014) 1993–1997.
[16] W. Ji, P. Zhao, T. He, X. He, A. Farooq, C.K. Law, On the controlling mechanism of the upper turnover states in the NTC regime, Combust. Flame 164 (2016) 294–302.
[17] P. Zhao, C.K. Law, The role of global and detailed kinetics in the first-stage ignition delay in NTC-affected phenomena, Combust. Flame 160 (2013) 2352–2358.
[18] D.G. Goodwin, R.L. Speth, H.K. Moffat, B.W. Weber, Cantera: an object-oriented software toolkit for chemical kinetics, thermodynamics, and transport processes. https://www.cantera.org, doi:10.5281/zenodo.1174508.
[19] T. Nagy, T. Turányi, Uncertainty of Arrhenius parameters, Int. J. Chem. Kinet. 43 (2011) 359–378.
[20] Y. Tao, H. Wang, Joint probability distribution of Arrhenius parameters in reaction model optimization and uncertainty minimization, Proc. Combust. Inst. 37 (2019) 817–824.
[21] D.A. Sheen, X. You, H. Wang, T. Løvås, Spectral uncertainty quantification, propagation and optimization of a detailed kinetic model for ethylene combustion, Proc. Combust. Inst. 32 (2009) 535–542.
[22] P.G. Constantine, E. Dow, Q. Wang, Active subspace methods in theory and practice: applications to Kriging surfaces, SIAM J. Sci. Comput. 36 (2014) A1500–A1524.
[23] P.G. Constantine, M. Emory, J. Larsson, G. Iaccarino, Exploiting active subspaces to quantify uncertainty in the numerical simulation of the HyShot II scramjet, J. Comput. Phys. 302 (2015) 1–20.
[24] W. Ji, Z. Ren, C.K. Law, Evolution of sensitivity directions during autoignition, Proc. Combust. Inst. 37 (2019) 807–815.
[25] W. Ji, J. Wang, O. Zahm, Y.M. Marzouk, B. Yang, Z. Ren, C.K. Law, Shared low-dimensional subspaces for propagating kinetic uncertainty to multiple outputs, Combust. Flame 190 (2018) 146–157.
[26] K.E. Niemeyer, C.-J. Sung, M.P. Raju, Skeletal mechanism generation for surrogate fuels using directed relation graph with error propagation and sensitivity analysis, Combust. Flame 157 (2010) 1760–1770.
[27] P.O. Mestas, P. Clayton, K.E. Niemeyer, {pyMARS} v1.1.0. doi:10.5281/zenodo.3401549.
[28] K.E. Niemeyer, C.-J. Sung, On the importance of graph search algorithms for DRGEP-based mechanism reduction methods, Combust. Flame 158 (2011) 1439–1443.
[29] S.L. Fischer, F.L. Dryer, H.J. Curran, The reaction kinetics of dimethyl ether. I: high-temperature pyrolysis and oxidation in flow reactors, Int. J. Chem. Kinet. 32 (2000) 713–740.
[30] H.J. Curran, S.L. Fischer, F.L. Dryer, The reaction kinetics of dimethyl ether. II: low-temperature oxidation in flow reactors, Int. J. Chem. Kinet. 32 (2000) 741–759.
[31] E.A. Tingas, D.C. Kyritsis, D.A. Goussis, Comparative investigation of homogeneous autoignition of DME/air and EtOH/air mixtures at low initial temperatures, Combust. Theory Modell. 21 (2017) 93–119.
[32] E.A. Tingas, D.C. Kyritsis, D.A. Goussis, Autoignition dynamics of DME/air and EtOH/air homogeneous mixtures, Combust. Flame 162 (2015) 3263–3276.